Materials Today Communications 35 (2023) 106357

Contents lists available at ScienceDirect

Materials Today Communications

journal homepage: www.elsevier.com/locate/mtcomm

Effect of stearic acid on the mechanical and rheological properties of PLA/HA biocomposites

Júlia Cé de Andrade [a,c,*], Fernando Cabral [a], Frank Jorg Clemens [c], Jaqueline Leite Vieira [d], Milena B.P. Soares [d], Dachamir Hotza [a,b], Márcio Celso Fredel [a,b]

[a] Ceramic and Composite Materials Research Group (CERMAT), Federal University of Santa Catarina (UFSC), 88040-900 Florianópolis, SC, Brazil
[b] Interdisciplinary Laboratory for the Development of Nanostructures (LINDEN), Federal University of Santa Catarina (UFSC), 88040-900 Florianópolis, SC, Brazil
[c] Laboratory for High-Performance Ceramics (LHPC), Empa - Swiss Federal Laboratories for Materials Science and Technology, Überlandstrasse 129, 8600 Düebendorf, Switzerland
[d] Gonçalo Moniz Institute, Oswaldo Cruz Foundation (FIOCRUZ), 40296-710 Salvador, BA, Brazil

ARTICLE INFO

Keywords:
Biocomposites
Bone tissue engineering
Scaffolds, polylactic acid
Nano-hydroxyapatite
Stearic acid
Biocompatible surfactants
Fused deposition modeling

ABSTRACT

In this study, biocomposite filaments of polylactic acid (PLA) combined with stearic acid (SA)-coated nano-hydroxyapatite (HA) filler were prepared and characterized. These filaments were then used in material extrusion (MEX) additive manufacturing via fused deposition modeling (FDM) to create scaffolds for bone tissue engineering (BTE). Initially, HA was characterized using transmission electron microscopy (TEM), X-ray diffraction (XRD), and the Rietveld method. Particle size distribution was examined through dynamic light scattering (DLS), and its specific surface area was determined by the Brunauer-Emmett-Teller (BET) method. Subsequently, the HA nanoparticles were coated with stearic acid (SA) to explore its potential as a surfactant for PLA/HA nanocomposites. For composite fabrication, pure HA and SA-coated HA were mixed with PLA in a torque rheometer to obtain PLA/HA and PLA/HA-SA biocomposites. Their flow behavior was evaluated using a slit die rheometer, demonstrating that the SA coating improved rheological properties. The composites were extruded to produce 1.75 mm diameter filaments, which were analyzed by mechanical tensile testing, showing that the SA coating reduced the fragility of the PLA/HA filaments. The filaments exhibited high repeatability in terms of quality, facilitating scaffold printing. The FDM-manufactured scaffolds were analyzed through compressive testing, Fourier transform infrared (FTIR) spectroscopy, differential scanning calorimetry (DSC), and AlamarBlue Cell Viability Analysis. The results demonstrated that these scaffolds possess the required mechanical, thermal, and cytotoxicity properties for applications in bone tissue engineering.

1. Introduction

Tissue engineering is an interdisciplinary field that applies concepts from engineering and life sciences to develop biological substitutes that restore, maintain or improve tissue functions [1]. Bone tissue engineering (BTE) aims to develop implants and prostheses that allow the regeneration of damaged bone tissue, resulting from a natural bone defect or bone loss, commonly due to tumors or fractures [2] The demand for biomaterials in BTE continues to grow, with the aim of restoring the structure and function of tissue to its natural state. Consequently, it is essential to develop implants that stimulate bone regeneration and are gradually absorbed by the body once their function is fulfilled [3].

Inspired by the nature of bone tissue, this study seeks to replicate conditions that foster bone growth by fabricating bone scaffolds produced by the additive manufacturing (AM) technique of fused deposition modeling (FDM). AM is applied to the repair of bone lesions because it can reproduce the complex geometry of the defects [4] and produce customized bone substitutes that imitate the mechanical, topological, and cellular properties of human tissue [2].

According to ASTM-I F2792 [5] AM is "a process of joining materials to make objects from 3D model data, layer upon layer"[6]. This means that a file generated from a 3D image is divided into horizontal layers, with each layer's characteristics defined based on specific requirements.

* Correspondence to: CERMAT – Ceramic and Composite Materials Research Group, Federal University of Santa Catarina, Campus Trindade, 88040-900 Florianópolis, SC, Brazil.
E-mail address: juliaceap@gmail.com (J. Cé de Andrade).

https://doi.org/10.1016/j.mtcomm.2023.106357
Received 1 March 2022; Received in revised form 30 May 2023; Accepted 1 June 2023
Available online 2 June 2023

This approach allows for the construction of complex architectures while eliminating the need for multi-stage processing. FDM is an extrusion-based AM technique that involves partially melting a thermoplastic polymer filament and extruding it layer by layer to form the final structure. This process allows for the creation of interconnected porous structures in an automated, organized, and reproducible manner [7].

Polylactic acid (PLA) and hydroxyapatite (HA) are biomaterials extensively used in FDM for medical and dental applications. It is interesting to combine the properties of polylactic acid reinforced with nano-hydroxyapatite aiming to associate the bioabsorbability of the polymer with the osteoconductivity of ceramics [8]. Although PLA/HA biocomposites provide recognized benefits, the polymer-ceramic interface exhibits limited compatibility, which can be improved by incorporating biocompatible surfactants, such as stearic acid (SA). This acid possesses both a polar functional end-group (O and H) and a non-polar hydrocarbon end-group (C and H), rendering it an ideal candidate for enhancing compatibility at the polymer-ceramic interface [9].

This study aims to optimize processing conditions to incorporate SA as a surfactant in PLA/HA nanocomposites aiming to improve its rheological and mechanical properties. The SA investigation endeavors to contribute to the ongoing research on developing cellular PLA/HA scaffolds with the potential to serve as implantable bone devices. Ultimately, this study aims to contribute to the development of high-performance bone scaffolds, intended to be capable of inducing and guiding new bone tissue growth at injury sites, effectively filling bone gaps resulting from trauma, degenerative disease, or tumors.

2. Materials and methods

Poly(lactic acid) (PLA, 3D850 NatureWorks) pellets were used as the composite matrix, while synthetic hydroxyapatite nanopowder (HA, Nanosynt, FGM Dental Products) was used as the nanofiller. Firstly, HA was characterized by scanning electron microscopy (SEM, Hitachi TM 3030), using gold-sputtered samples, at 10 kV and a magnification of 500 X. Transmission electron microscopy (TEM, JEOL JEM-1011) was then used to examine samples prepared in a copper network with a carbon conductive film. X-ray diffraction (XRD, D2 Phaser, Bruker) was applied at 100 kV, allowing an expansion of 200,000 X (Cu-Kα radiation was fixed at $\lambda = 1.54184$ Å, operating at a power of 30 kV and 10 mA).

2.1. Characterization of HA nanoparticles

The measurements were carried out using Bragg-Brentano geometry (θ-2θ) within a range of 5–80° and a step size of 0.05° [10]. Crystallinity was evaluated through X-ray diffraction (XRD), considering the ratio of the crystalline peak area to the combined area of crystalline and amorphous peaks [10]. Subsequently, the Rietveld method was applied to refine the results by optimizing structural parameters [11]. The particle size distribution was examined via dynamic light scattering (DLS) with a Zetasizer Nano ZS (ZEN 3600, Malvern Panalytical), using a 0.3 wt% hydroxyapatite (HA) aqueous suspension [12]. Lastly, the specific surface area was determined by employing the Brunauer-Emmett-Teller (BET) method for nitrogen adsorption, following the ASTM D 6556 standard [13,14].

2.2. Coating of HA nanoparticles with stearic acid

Additionally, HA nanoparticles were coated with the surfactant stearic acid (SA, 95% Sigma-Aldrich) to enhance the polymer-ceramic interface. This process involves mixing HA powder with SA for 18 h, using toluene as a solvent, in a jar-turning mill with zirconia spheres. It is important to notice that these zirconia spheres were only used to improve homogenization and were not incorporated into the composition itself. After the mixing, the solvent was extracted using a rotational evaporator for 5 h. Finally, the coated hydroxyapatite powder was sieved for 30 min, resulting in the SA-coated nano-hydroxyapatite. The rheological properties were measured before and after the HA coating using a torque rheometer (Haake MiniLab, Thermo Scientific).

2.3. Composites preparation

PLA/HA and PLA/HA-SA nanocomposites were prepared by mixing PLA with HA, and with SA-coated HA, respectively. Aiming to define the ideal parameter set for producing PLA/HA and PLA/HA-SA nanocomposites, the materials were mixed in a modular torque rheometer (Haake PolyLab QC, Thermo Scientific) for 15 min, varying two levels of temperature, rotational speed, and filler percentage (175 and 190 °C; 60 and 100 rpm; 5 and 10 wt%) obtaining 16 different composite combinations (8 for PLA/HA and 8 PLA/HA-SA).

2.4. Composites characterization

Employing a 2^4 complete factorial design without repetition, the 16 composites were subjected to rheological analysis to assess the effect of the process parameters and the SA coating on torque and viscosity. The processing parameters (time, temperature, rotational speed, and HA quantity) were treated as factors, while the asymptotic torque served as the independent variable. The torque was studied from the mixing process, and the viscosity measurements were performed with a concentric cylinder rheometer (MiniLab II, Haake, Thermo Scientific). The PLA/HA and PLA/HA-SA compositions that showed more suitable rheological properties were selected for producing BTE filaments and scaffolds.

2.5. Filaments preparation

PLA/HA and PLA/HA-SA composites selected in the characterization section (10 wt% filler 100 rpm 190 °C) were ground using a knife mill and subsequently melt extruded (Mini Extruder Lab-16, AX Plastics) to produce continuous filaments of 1.75 mm in diameter. The extrusion temperature was maintained at 190 °C, and low rotational speed was employed to prevent polymer degradation.

2.6. Filaments characterization

The filaments were evaluated by uniaxial tensile testing using a tensile tester (Emic 23–5 S) equipped with a 500 N load cell, a crosshead speed of 0.5 mm/min, and a grip separation of 50.2 mm.

2.7. Scaffolds preparation

The filaments were employed as feedstock to fabricate 30 scaffolds (10 pure PLA, 10 PLA/HA, and 10 PLA/HA-SA) by FDM (Minibot 130 printer) with a 0.3 mm diameter nozzle. Scaffold geometry was designed using SolidWorks software (Dassault Systèmes), and filling variations were chosen with slicer software (Simplify3D) to maintain a pore size of approximately 200 μm and achieve optimal surface quality. Both pore size and surface quality are critical factors for proper cell integration and growth. All 30 scaffolds, measuring 3 × 3 cm (diameter × height), were printed with "open porosity" in order to promote cellular interaction. However, open porosity may compromise mechanical properties compared to dense structures [13,14]. Another significant geometric consideration is the vertical overlap of scaffold layers, which prevents bone cells from infiltrating the scaffold structure [14].

2.8. Scaffolds characterization

The composites were characterized by Fourier-transform infrared (FTIR) spectroscopy (PerkinElmer Frontier). FTIR spectra were obtained at wavenumbers of 4000–400 cm^{-1}, through the accumulation of 32 scans, with an analysis interval of 4 s. Differential scanning calorimetry

(DSC, PerkinElmer 6000) with cycles of 30–230 °C and a heating rate of 10 °C/min to evaluate the influence of the HA particles on the thermal properties. The compression test was performed with a texturometer (TA.HDplus, Stable Micro Systems) with a 750 kg load cell, 60% sample compression, a 35 mm cylindrical probe, and a test speed of 0.75 mm/s.

The cytotoxicity of SA was examined using the AlamarBlue assay (Invitrogen, Carlsbad, CA, USA). This assay serves as an indicator of cell metabolic activity and proliferation, which can be correlated with cell viability, as metabolically active cells are able to convert resazurin salt and are considered healthy and viable. Murine fibroblasts L929 were cultured in Dulbecco's Modified Eagle Medium (DMEM; Life Technologies, GIBCO-BRL) enriched with 10% fetal bovine serum (FBS; GIBCO, Thermo Fisher Scientific) and 1% penicillin/streptomycin (Thermo Fisher Scientific). Cells were maintained in a 5% CO2 incubator at 37 °C before conducting the in vitro cell test. The scaffolds were sterilized using UV light for 1 h and then placed in a 24-well plate, submerged in the culture medium. After 24 h, the culture medium was removed, and the cells were seeded onto the scaffolds at a density of 5 × 105 cells/well. The cells were incubated for 48 h alongside the scaffold at 5% CO2 and 37 °C. Following incubation, resazurin sodium salt reagent was added to each well at a 10% v/v concentration and incubated for an additional 4 h. Subsequently, the supernatant was collected and transferred to a 96-well plate. The metabolic activity of the cells was determined by measuring the reaction product using a multi-plate reader at 570 and 600 nm wavelengths. All experiments were conducted in triplicate, with control wells containing only cells and no scaffolds [15–17].

2.9. Data analysis

Data analysis and curve fitting for the torque data were done using the Levenberg-Marquardt algorithm available in Origin® (Trial Version, OriginLab Corporation). For the composites preparation and rheological analysis, the experiments were performed using a 2^4 complete factorial design with no repetition. Temperature (T), rotational speed (RS), weight percentage of hydroxyapatite (%HA), and addition of stearic acid (SA) as factors and asymptotic torque as an independent factor. Furthermore, a 2^3 factorial design (T, %HA, and addition of SA) with repetition was performed. The analysis of the effect of factors and their interactions was carried out using Excel (Student Edition, Microsoft) and RStudio (Integrated Development for R. RStudio, PBC). All statistical tests used a 0.05 level of significance.

3. Results and discussion

3.1. Analysis of HA and HA-SA coated nanoparticles

Fig. 1(a) displays the characteristic peaks of HA, identified by JCPDS 9–432. The sample exhibits a degree of crystallinity of 86% with a crystalline peak area of 4340 and a total area of 5041. The literature reports that crystallinity above 70% results in higher biocompatibility [18]. From the XRD spectrum, Rietveld's method was applied to obtain a simulated diffractogram. After identifying the HA phase (89–6439), the database card was selected from the ICSD database [19]. The simulated standard was obtained by Rietveld refinement (Fig. 3(b)) through the following steps: background, network parameters, beta isotropic/anisotropic, atom coordinates, and instrumental factors. At the end of the refinement, the weighted profile R-factor (Rwp) and goodness of fit (GoF) measured 13.14 and 1.16, respectively. The lattice parameters a, b, and c for the hexagonal structure of HA are shown in Table 1. The ICSD database parameters are also displayed for comparison, hence, the values obtained are in agreement with ICSD 87670 [19].

HA exhibits a specific surface area of 16 m^2/g, as determined by the Brunauer-Emmett-Teller (BET) method. Particle size measurements revealed values of 150 ± 19 nm and 230 ± 9 nm for pure HA, and SA-coated samples, respectively. SA has been widely used as a surfactant and anti-agglomeration agent enhancing the flow properties of composites containing calcium phosphates, such as HA [20,21] The current study demonstrates that coating HA particles with SA results in an increase in particle size while reducing the size of agglomerates. Light scattering measurements reveal an agglomerates size of 380 nm in SA-coated samples and 575 nm in non-coated samples.

Fig. 2 presents transmission electron micrographs (TEM) of HA particles with and without SA coating allowing the visualization of the size and shape of agglomerates. Larger agglomerates are observed in samples without coating. The analysis of TEM images reveals that the

Table 1
Lattice parameters for HA after Rietveld refinement and ICSD database:.

Lattice parameter	Experimental (Å)	ICSD 87670 (Å)
a	9.41	9.42
b	9.41	9.42
c	6.88	6.88

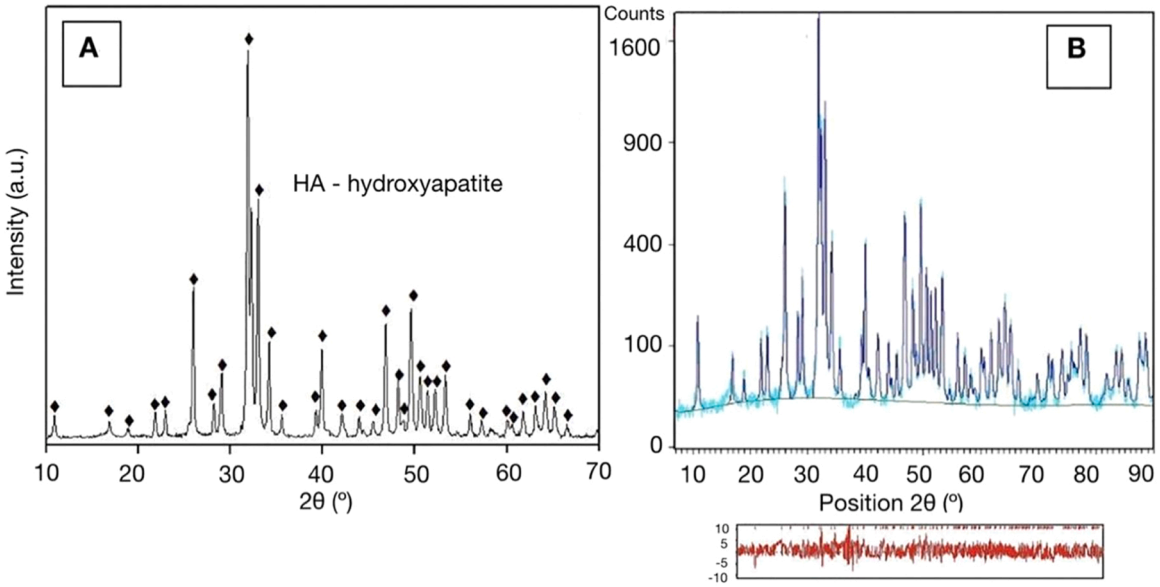

Fig. 1. XRD analysis of (a) HA filler, (b) Rietveld refinement for the HA filler with simulated (blue), and residual diffractograms (red).

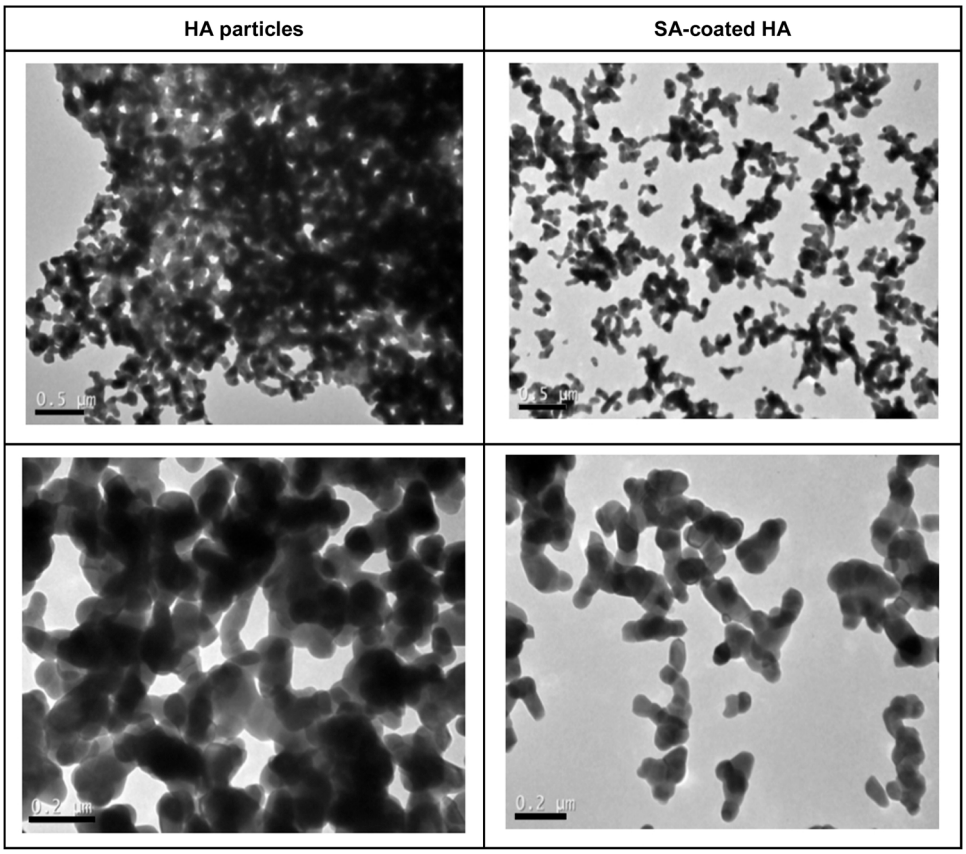

Fig. 2. TEM images of HA particles (left) and SA-coated HA particles (right).

majority of agglomerates in SA-coated samples fall within the range of 300–400 nm, whereas those in non-coated samples measure up to 700 nm, confirming that the incorporation of SA effectively reduces agglomerate size.

3.2. Analysis of PLA/HA and PLA/HA-SA composites

The Equilibrium Torque Analysis for the composites is presented in Fig. 3, which shows the compounding process within the rheometer, illustrating torque as a function of time for both PLA/HA-SA and PLA/HA across eight variable combinations. The sharp decrease in torque values is a characteristic of the homogenization process during mixing. When the torque becomes constant, further homogenization cannot be achieved, and, statistically, mixing and demixing of the two phases are in equilibrium [22]. Thus, the equilibrium region is the area of interest in this study. In this region, the torque as a function of time was analyzed by the Levenberg Marquardt method with a decreasing exponential fitting, with R^2 greater than or equal to 0.99.

Table 2 shows the results for the analysis of variance with 4 factors (temperature, rotational speed, weight percentage of HA, and addition

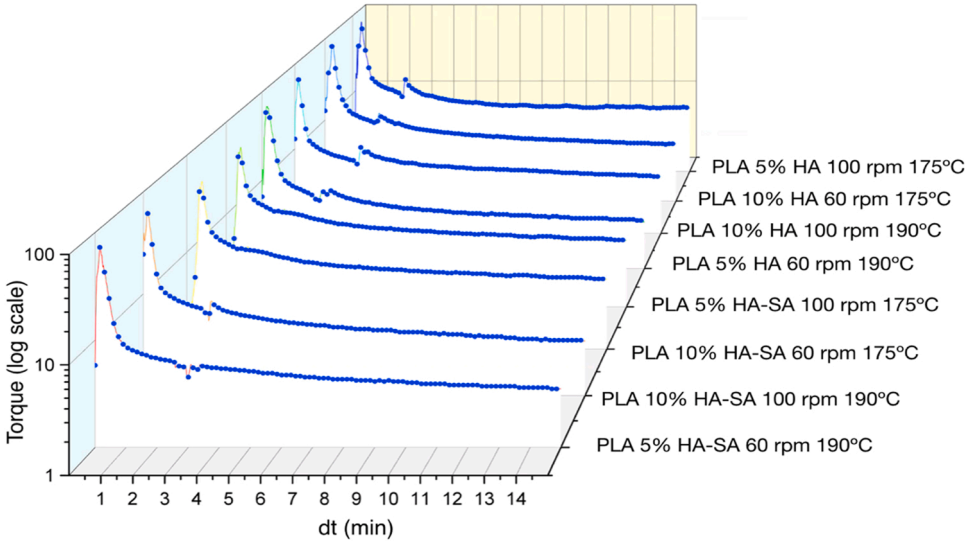

Fig. 3. Torque (logarithm scale) as a function of time, for 8 feedstock combinations: % HA, rotational speed, and temperature.

Table 2
Results obtained in the analysis of variance with 4 factors and 2 levels without repetition showing the estimate of effects for the factors hydroxyapatite(HA) weight percentage (%HA), temperature (T), stearic acid (SA), and rotational speed (RS) on the equilibrium torque with respective proportions of variance. The results of the analysis of variance with 3 factors (T, %HA, and addition of SA) with repetition are shown in the last column (p values). A * indicates that the factor is statistically significant.

Factors and interactions	Estimate of Effect	Proportion of variance	p value
T	-2.249	0.614	$< 10^{-4}$*
SA	-1.498	0.273	$< 10^{-3}$*
%HA	0.295	0.011	0.33
%HA × T	0.310	0012	0.31
T × SA	0.096	0.001	0.75
%HA × SA	-0.293	0010	0.34
%HA × T × SA	-0.014	$< 10^{-4}$	0.96
RS	0.064	0.0005	—
%HA × T × RS	0.513	0.032	—

of SA as factors) with two levels with 16 measurements for the equilibrium torque as the dependent variable. From the results of this 24 without repetition experimental design, it is possible to infer that the factors that most influence the equilibrium torque are temperature and coating with SA, with a dominant influence of the temperature.

These two factor account for 87% of the variability in the asymptotic torque. Higher temperature (low value of 175 0 C and high value of 190 0 C) and the presence of SA both reduce the asymptotic torque. The amount of HA (low value of 5% and high value of 10%) has no significant effect on the equilibrium torque.

The rotational speed in the range of the experiment (low value of 60 rpm and high value of 100 rpm) showed no effect on the asymptotic torque, with a proportion of variance of 5 × 10–4. In addition, the largest calculated effect of an interaction involving the rotational speed (%HA × T × RS) is 4.4 times lower than the effect of the temperature with a proportion of variance of 0.032. This indicates that rotation speed and all its interaction effects are negligible and can be included in the error term reducing the design to a 23 design with 16 measurements. HA is kept as a factor due to its bio-integration importance. A significance level of 0.05 was used.

The last column in Table 2 presents p values for factors and interactions for the design with 3 factors. As expected, only the temperature and coating have a significant effect on the asymptotic torque. The p values for the weight percentage of HA and its interactions show that this factor does not influence the asymptotic torque. It is important to note that higher torque indicates greater flow resistance and higher viscosity. These results confirm that coating with SA reduces the equilibrium torque and should reduce the viscosity of the samples.

As for the viscosity analysis of the composites, the flow behavior is strongly affected by the presence of SA. As expected from the analysis of variance results, the use of SA as a surfactant leads to lower viscosity. For both feedstocks, a shear thinning effect (decrease in viscosity as the shear rate increases) was observed. Viscosity as a function of shear rate can be described by the Ostwald-de Waele Model $\eta = K^{n-1}$.

In this power-law model, η is the viscosity (Pa·s); K is the flow consistency index (Pa·s), related to the stiffness of the feedstock (the higher the K value the higher the viscosity of the feedstock will be); n is the power law constant (unitless), related to the pseudoplasticity (the closer n is to zero the stronger the shear thinning effect will be); and γ refers to the shear rate (s^{-1}). The values for K and n are shown in Table 3, along with the R^2 values for the fitted data. It has been observed in previous studies that the SA reduces inter-particle friction, which can be seen in the reduction of the viscosity at higher shear rates [23].

Table 3
K, n, and R^2 obtained from the fitting of the rheology curves.

Sample	K (Pa·s)	n	R^2
10% HA (100 rpm / 190 °C)	346.83	0.613	0.92
10% HA-SA (100 rpm / 190 °C)	104.80	0.685	0.95

In this rheological investigation, only the presence or absence of coating with SA alters significantly the behavior of the composites. Fig. 4 shows the curve viscosity versus shear rate for the 10% HA samples (100 rpm/190 °C) with and without SA coating. For the temperature chosen, coating with SA reduced the viscosity by almost 50% for all shear rate values. Coating with SA reduced significantly the flow consistency index. This confirms previously reported findings [3], where the addition of SA reduced the particle friction, which reduces the viscosity at higher shear rates.

3.3. Analysis of PLA/HA and PLA/HA-SA filaments

The mechanical analysis of the filaments shows values for the average tensile strength of the composites with and without coating were 46 MPa and 44 MPa, respectively. The average Young's modulus values calculated from the linear regression between points 1 and 2.5 mm/mm (% deformation) were 9 MPa for samples with coating and 75 MPa for samples without coating with stearic acid.

Based on the stress-strain curves shown in Fig. 5, it can be concluded that coating with SA produces fewer brittle filaments, which can lead to better mechanical properties of scaffolds for tissue engineering. Appropriate mechanical properties are also vital to ensure long-term structural and functional viability in vivo [24] and are determining factors in directing cellular activity [25,26].

3.4. PLA/HA and PLA/HA-SA scaffolds characterizations

The Fourier transform infrared (FTIR) spectroscopy curves in Fig. 6 represent PLA, PLA/HA, and PLA/HA-SA samples. Considering the chemical composition of the PLA, there are characteristic peaks of the CH (2960 cm^{-1}), C = O (1720 cm^{-1}), and CO (1120 cm^{-1}) and between 3600 and 3000 cm^{-1} related to the presence of OH bonds [27].

It is also possible to notice undulation between 3600 and 3000 cm^{-1} related to the OH bonds in the HA. The addition of SA did not show significant changes in the characteristic peaks of PLA and HA composites, indicating that the percentage of SA added to the samples did not affect the chemical structure of the materials.

Fig. 7 shows the curves for PLA, PLA/HA, and PLA/HA-SA obtained during the second heating cycle of the differential scanning calorimetry (DSC) analysis. It is possible to observe that the Tg value is approximately 65 for PLA and 69 °C for PLA/HA and PLA/HA-SA and that

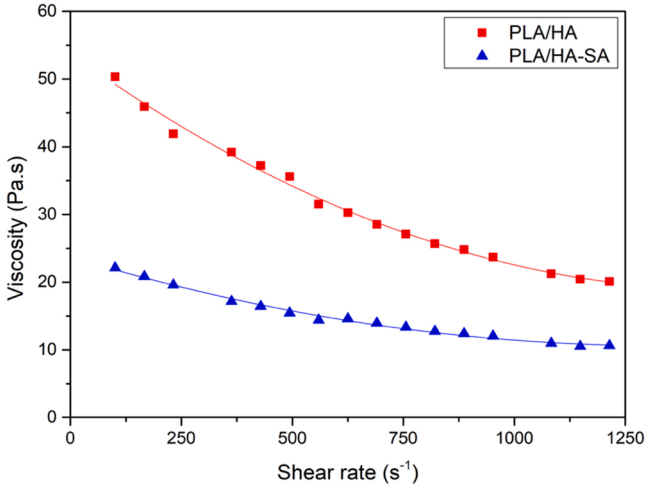

Fig. 4. Viscosity as a function of shear rate for PLA/HA and PLA/HA-SA. The solid line shows the fitted curve obtained using the power law equation ($\eta = K\gamma^{n-1}$).

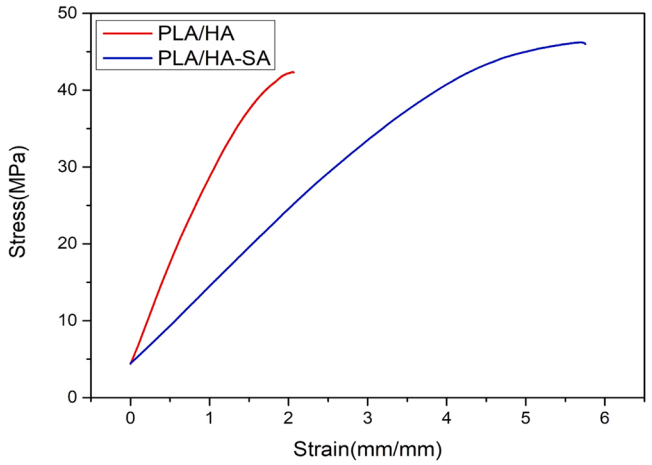

Fig. 5. Stress-strain curves for filaments of PLA/HA (red) and PLA/HA-SA (blue) obtained from tensile testing.

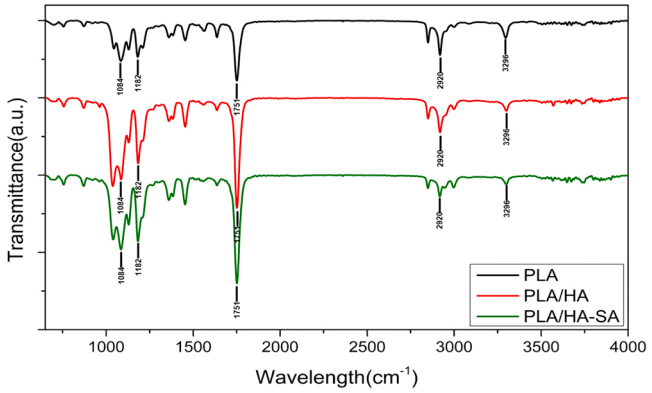

Fig. 6. FTIR spectroscopy curves for PLA, PLA/HA, and PLA/HA-SA scaffolds.

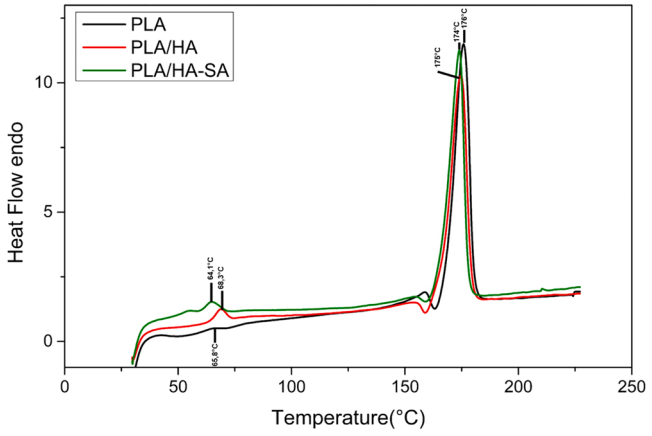

Fig. 7. DSC curves for PLA, PLA/HA, and PLA/HA-SA scaffolds.

melting occurs at approximately 175 °C for all samples. Damadzadeh et al. studied the effect of ceramic fillers on PLA thermal properties referring to no change in Tg and a slight increase of Tm when adding HA to PLA composites in higher percentages, possibly related to the stress release of molecular chains during the heating process [28]. Nevertheless, for the percentage studied in this work, the addition of both HA and SA did not show significant changes in the characteristic peaks of pure PLA, indicating that for the compositions studied, the fillers did not affect significantly the thermal behavior.

Fig. 8 represents the stress-strain curves of the compression tests performed in PLA/HA and PLA/HA-SA scaffolds. The tests were performed in three different samples for each group, but the figures show an average curve. It can be observed that the PLA/HA curves present a more fragile behavior than PLA/HA-SA, even though samples show similar compressive strength of 45 MPa on average, they show a significant difference in Young Modulus, in average 56 MPa for non-coated samples, and 7 MPa for coated ones. In agreement with literature that affirms coated HA should present better mechanical properties than non-coated samples [29].

3.5. *Cytotoxicity analysis of PLA/HA and PLA/HA-SA scaffolds*

The AlamarBlue assay results, depicted in Fig. 9, demonstrate that none of the analyzed scaffolds exhibited significant cytotoxicity. As the biocompatibility of PLA and PLA/HA scaffolds has already been established in the literature [15,16,30,31], this pattern was anticipated for the scaffolds without the SA. It is possible to notice that the results obtained from the scaffolds containing the SA were similar to those without it, exhibiting a nontoxic behavior. The control in this assay refers to cell cultures without any scaffold present. Consequently, the scaffolds exhibited favorable properties for additional biological applications.

4. Conclusions

Porous scaffolds with promising mechanical, rheological, and biocompatible characteristics for bone tissue engineering (BTE) applications can be fabricated using fused deposition modeling (FDM) with 1.75 mm diameter PLA/HA and PLA/HA-SA filaments. The HA used in this study was found to be suitable for application in bone tissue engineering, due to the morphological characteristics evidenced through TEM, XRD, zeta sizer, and specific surface area results. Based on rheological tests carried out with a torque rheometer, the composite processing conditions were optimized and the production parameters were defined as 10% HA-SA filler at 100 rpm and 190 ºC.

Coating HA particles with SA showed promising results, reducing the formation of agglomerates and enhancing the dispersion of ceramic particles. For the powder stage, the coating increased the particle size but reduced the size of the agglomerates. For the mixing stage, coating with SA decreased the maximum and equilibrium torque and decreased the viscosity due to less friction. The temperature during mixing also affects the rheological properties and is an important factor in the manufacturing process. For the filaments, SA coating reduced fragility. For the scaffolds, the SA-coating reduced the fragility yielding a smaller Young's modulus, while did not interfere significantly with the thermal

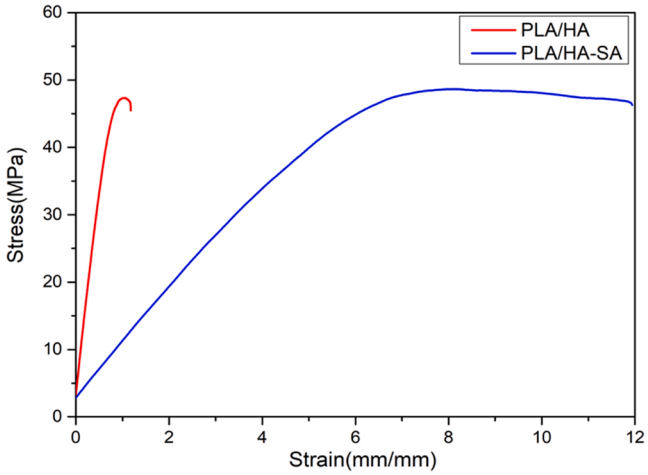

Fig. 8. Stress-strain curves for scaffolds of PLA/HA (red) and PLA/HA-SA (blue) obtained from compressive testing.

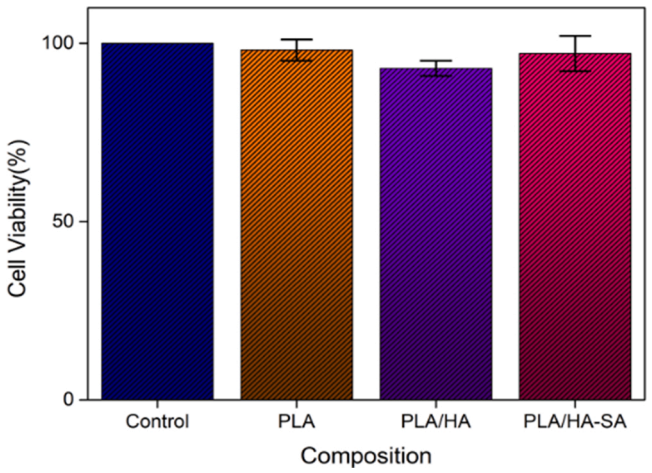

Fig. 9. Result of the AlamarBlue assay, presenting absence of cytotoxic effect in the treated cells. Graph showing the metabolic response of L929 cell cultured with different scaffolds in the well (PLA, PLA/HA, and PLA/HA-SA scaffolds) for 48 h, indicating the cell viability even in the presence of the scaffold printed with SA.

properties, and exhibited no significant cytotoxicity.

In conclusion, we can state that SA is a promising surfactant for PLA/HA composites as the reduction in HA agglomerate size improves the dispersion of the ceramic particles, which is a major factor for BTE applications. This improvement can lead to scaffolds with good mechanical properties while maintaining suitable biocompatibility. In future research, it is important to investigate the in vitro degradation and cell differentiation of the scaffolds.

CRediT authorship contribution statement

Júlia Cé de Andrade Pinto: Writing, Conceptualization, Methodology, Writing – original draft. **Fernando Cabral:** Data curation, Statistics and Reviewing. **Frank Jorg Clemens**: Rheology Tests and Reviewing. **Dachamir Hotza:** Supervision, Writing – review & editing. **Márcio Celso Fredel**: Supervision, Writing – review & editing.

Declaration of Competing Interest

The authors declare that they have no known competing financial interests or personal relationships that could have appeared to influence the work reported in this paper.

Data Availability

Data will be made available on request.

Acknowledgments

The authors wish to thank the CNPq and CAPES for the financial assistance that enabled this work, and the FGM Dental Group company for providing the hydroxyapatite used in this study.

References

[1] J.P. Vacanti, R. Langer, Tissue engineering: the design and fabrication of living replacement devices for surgical reconstruction and transplantation, Lancet (1999).
[2] N.J. Castro, R. Patel, L.G. Zhang, Design of a Novel 3D printed bioactive nanocomposite scaffold for improved osteochondral regeneration, Cell Mol. Bioeng. (2015).
[3] C. Esposito Corcione, F. Scalera, F. Gervaso, F. Montagna, A. Sannino, A. Maffezzoli, One-step solvent-free process for the fabrication of high-loaded PLA/HA composite filament for 3D printing, J. Therm. Anal. Calor. 134 (1) (2018) 575–582.
[4] I. Zein, D.W. Hutmacher, K.C. Tan, S.H. Teoh, Fused deposition modeling of novel scaffold architectures for tissue engineering applications, Biomaterials (2002).
[5] ASTM, Standard Terminology for Additive Manufacturing Technologies (ASTM F2792 - 12a), ASTM International, 2012.
[6] Technologies M. , 2016. StandardTerminology for. 2016;5–7.
[7] Y. Ramot, M. Haim-Zada, A.J. Domb, A. Nyska, Biocompatibility and safety of PLA and its copolymers, Adv. Drug Deliv. Rev. (2016).
[8] P. Gentile, V. Chiono, I. Carmagnola, P.V. Hatton, An overview of poly(lactic-co-glycolic) Acid (PLGA)-based biomaterials for bone tissue engineering, Int. J. Mol. Sci. Vol. 15 (2014).
[9] A. Bellini, S. Güçeri, Mechanical characterization of parts fabricated using fused deposition modeling, Rapid Prototyp. J. [Internet] 9 (4) (2003) 252–264, https://doi.org/10.1108/13552540310489631.
[10] Smith D.K., Fiala J., Ryba E. Book Reviews - The Rietveld Method, R. A. Young, Editor, IUCr Monographs in Crystallography, 5, International Union of Crystallography, Oxford University Press, New York, NY, pp. 298. - The Rietveld Method, R. A. Young, Editor, Oxford University Press, Ox. Powder Diffr. 1993;
[11] H.M. Rietveld, The Rietveld method, Phys. Scr. 89 (9) (2014).
[12] C.S.S.R. Kumar, Nanosystem characterization tools in the life sciences, Nanotechnologies life Sci. 3 (2006).
[13] S. Brunauer, P.H. Emmett, E. Teller, Adsorption of gases in multimolecular layers, J. Am. Chem. Soc. 60 (2) (1938).
[14] ASTM International, Standard Test Method for Carbon Black - Total and External Surface Area by Nitrogen Adsorption. Designation: D6556 – 10 Standard, i, ASTM International, 2012, pp. 1–5 (Available from:), ⟨http://www.biochar-international.org/sites/default/files/ASTMD6556-10N2BETforCarbonBlack.juhu2739.pdf⟩.
[15] L. Macêdo Ferreira Santos, B. de, Cardim Barreto, H. Costa Quadros, C. Santana Meira, R. Siqueira Ferraz-Carvalho, de, Souza, J. de Rebouças, et al., Tissue response and retention of micro- and nanosized liposomes in infarcted mice myocardium after ultrasound-guided transthoracic injection, Eur. J. Pharm. Biopharm. (2022) 173.
[16] A. Iglesias-Mejuto, C.A. García-González, 3D-printed alginate-hydroxyapatite aerogel scaffolds for bone tissue engineering, Mater. Sci. Eng. C. (2021) 131.
[17] H. El-Hamshary, M.E. El-Naggar, A. El-Faham, M.A. Abu-Saied, M.K. Ahmed, M. Al-Sahly, Preparation and characterization of nanofibrous scaffolds of ag/vanadate hydroxyapatite encapsulated into polycaprolactone: morphology, mechanical, and in vitro cells adhesion, Polymers 13 (8) (2021).
[18] M. Hellenbrandt, The inorganic crystal structure database (ICSD) - Present and future, Crystallogr. Rev. (2004).
[19] J.W. Nam, M.Y. Kim, S.J. Han, Cranial bone regeneration according to different particle sizes and densities of demineralized dentin matrix in the rabbit model, Maxillofac. Plast. Reconstr. Surg. 38 (1) (2016) 1–16.
[20] Y. Li, W. Weng, Surface modification of hydroxyapatite by stearic acid: Characterization and in vitro behaviors, J. Mater. Sci. Mater. Med 19 (1) (2008) 19–25.
[21] Gonsalves JKMC, J.N.S. Ferro, E.O. Barreto, R.S. Nunes, M.E.G. Valerio, Influence of concentration of hydroxyapatite surface modifier agent on bioactive composite characteristics, Ceram. Int. 42 (15) (2016) 17023–17031.
[22] M. Salehi, E.M. Pfaff, A. Kaletsch, T. Graule, F. Clemens, B. Grobéty, Manufacturing of tubular dead-end membranes by continuous thermoplastic extrusion, Int. J. Appl. Ceram. Technol. 12 (S2) (2015) E13–E18.
[23] L. Gorjan, L. Reiff, A. Liersch, F. Clemens, Ethylene vinyl acetate as a binder for additive manufacturing of tricalcium phosphate bio-ceramics, Ceram. Int. 44 (13) (2018) 15817–15823.
[24] B.P. Chan, K.W. Leong, Scaffolding in tissue engineering: General approaches and tissue-specific considerations, Eur. Spine J. 17 (SUPPL. 4) (2008).
[25] V. Kononenko, M. Narat, D. Drobne, Nanoparticle interaction with the immune system, Arh. Hig. Rada Toksikol. 66 (2) (2015) 97–108.
[26] M. Ahamed, M. Karns, M. Goodson, J. Rowe, S.M. Hussain, J.J. Schlager, et al., DNA damage response to different surface chemistry of silver nanoparticles in mammalian cells, Toxicol. Appl. Pharm. 233 (3) (2008) 404–410.
[27] M.K.M. Haafiz, A. Hassan, Z. Zakaria, I.M. Inuwa, M.S. Islam, M. Jawaid, Properties of polylactic acid composites reinforced with oil palm biomass microcrystalline cellulose, Carbohydr. Polym. (2013).
[28] B. Damadzadeh, H. Jabari, M. Skrifvars, K. Airola, N. Moritz, P.K. Vallittu, Effect of ceramic filler content on the mechanical and thermal behaviour of poly-l-lactic acid and poly-l-lactic-co-glycolic acid composites for medical applications, J. Mater. Sci. Mater. Med 21 (9) (2010 15) 2523–2531.
[29] S. Cheng, L. Chen, Y. Hong, G. Song, H. Liu, G. Tang, Surface modification of hydroxyapatite and its influences on the properties of poly(lactic acid)-based porous scaffolds, Fuhe Cailiao Xuebao/Acta Mater. Compos. Sin. 35 (5) (2018).
[30] J. Liuyun, X. Chengdong, J. Lixin, X. Lijuan, Effect of hydroxyapatite with different morphology on the crystallization behavior, mechanical property and in vitro degradation of hydroxyapatite/poly(lactic-co-glycolic) composite, Compos Sci. Technol. 93 (2014) 61–67.
[31] C. Xie, X. Lu, K. Wang, H. Yuan, L. Fang, X. Zheng, et al., Pulse electrochemical driven rapid layer-by-layer assembly of polydopamine and hydroxyapatite nanofilms via alternative redox in situ synthesis for bone regeneration, ACS Biomater. Sci. Eng. (2016).